COMPARING ACTIVE CONTOURS FOR THE SEGMENTATION OF BIOMEDICAL IMAGES

Birgit Möller and Stefan Posch

Institute of Computer Science, Martin Luther University Halle-Wittenberg
Von-Seckendorff-Platz 1, 06120 Halle (Saale), Germany

ABSTRACT

Application of active contours for image segmentation raises the question of contour representation, i.e. whether to use snakes or level sets. The representation directly affects issues like topology-preservation and energy optimization. In this paper we aim to contribute to the understanding of specific characteristics of contour representations with a detailed comparison of snakes vs. non-PDE level sets. Based on the same energy functional and applied to different kinds of real-world data our experiments show minor differences in segmentation quality, but outline important distinctions regarding implementation, parameter settings and computational effort.

Index Terms— Snakes, non-PDE level sets, comparison

1. INTRODUCTION

Active contours have become a popular technique for image segmentation in various domains over the last two decades since the publication of the seminal papers [1] and [2]. The underlying idea of these methods is to minimize an appropriate energy functional. This energy comprises a data term, also called external energy, and typically a regularizer or internal energy which depends exclusively on the shape of the contour(s). The choice of this energy depends heavily on the images considered and on the aim of the segmentation task.

Active contours are distinguished into snake and level set methods. Snakes explicitly represent a contour by a parametric curve, where as level sets use an implicit representation as the zero level of an embedding function. Despite the common idea of both techniques to minimize a given energy functional, they differ considerably with regard to the capacity to handle multiple objects, the ability to change or preserve topology, the optimization techniques including numerical stability, as well as computation time and implementational effort. Consequently to efficiently apply such techniques to segmentation problems from a specific domain it is fundamental to develop understanding and experience for the characteristics of different active contour approaches and their behaviors.

The main intention of this paper is to contribute to this understanding by directly comparing one snake and one non-PDE level set approach for two segmentation problems in microscopy images from the biomedical domain [3, 4]. In contrast to [5] for both techniques the same energy functional based on the Chan-Vese energy [6] is used, which is region-based in contrast to edge-based energies considered in [5]. To provide practically meaningful results original images from biomedical applications are used in the experiments, and besides qualitative and quantitative results also implementation issues and computation times are analyzed in detail.

2. RELATED WORK

Active contours date back to the pioneering work of [1] where snakes where introduced for energy-based image segmentation. The inherent nature of snakes impedes topological changes during segmentation. Although in [7] an approach to overcome this limit was presented, snakes are typically used in topology-preserving contexts [8, 9]. Regarding biomedical applications often multiple objects per image have to be segmented. To this end energy functionals hampering snake overlap have been developed [10]. Also geometric post-processing of snakes to eliminate self-overlap is often required. The model of explicit snake segmentation defines a PDE problem which is usually solved by iterative gradient-descent [1]. Due to numerical issues that sometimes occur , greedy optimization techniques were proposed [11], and level sets have gained increasing importance and wide-spread use due to their advantageous numerical properties.

As for snakes the prevailing approach for optimization of level sets is to use Euler-Lagrange equations to derive an iterative solution of the underlying variational problem (e.g. [2, 6]). The associated questions of time constants, re-initialization, and computation times can be bypassed by the direct non-PDE method proposed in [12] to minimize the energy. Pursuing a greedy approach, for each pixel the phase is changed if this decreases the global energy. Especially if this energy difference can be evaluated locally as for the Chan-Vese (CV) fitting term, this optimization strategy often yields a very fast scheme. Level set representations inherently allow to change the topology, e.g. to split or merge contours. However, this is of disadvantage in applications where the number and approximate position of objects to segment is given or determined by an initialization phase. A topology preserving scheme based on topological numbers was proposed in [13] which we adopted to the non-PDE

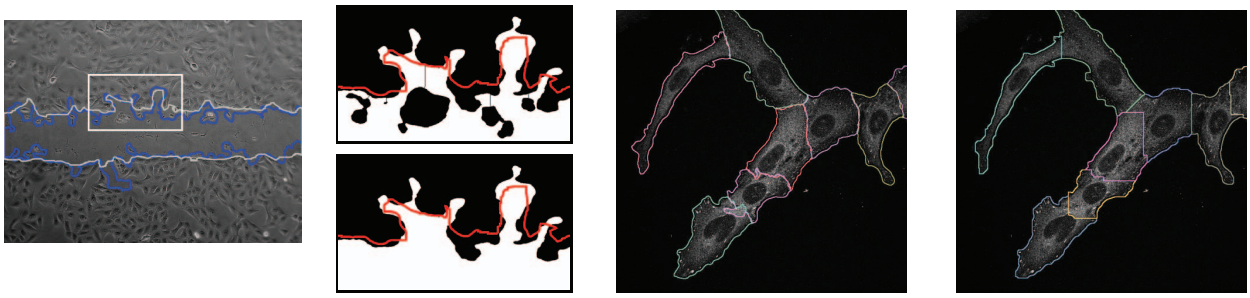


Fig. 1. From left to right images (contrast enhanced) and segmentation results are shown: (i) A scratch assay image with the final snake contour in dark grey (coloured version: blue) and the expert ground-truth in light gray; (ii) the level set result for a region of the left image (cf. to white rectangle) before (top) and after (bottom) post-processing, overlaid with the corresponding ground-truth contour in light grey (coloured version: red); (iii) snake and (iv) level set results for a sample cell image.

method in previous work [3]. Application of PDE level sets include the segmentation of leukocyte in microscopic images where both the CV fitting energy and an edge-based term are employed [14]. Cell segmentation in time-lapse fluorescence microscopy images in [15, 16] uses the CV energy with both the non-PDE and the PDE level set optimization.

3. METHODS

For our experiments we employ the commonly used CV energy [6]. In a level set framework it is given as

$$E(\phi, c_{fg}, c_{bg}) = \lambda_f \int_\Omega |I(\vec{x}) - c_f|^2 H(\phi(\vec{x}))d\vec{x} + \lambda_b \int_\Omega |I(\vec{x}) - c_b|^2 (1 - H(\phi(\vec{x})))d\vec{x} + \mu \int_\Omega |\nabla H(\phi(\vec{x})|d\vec{x},$$

where ϕ denotes the level set function and H the heaviside function. c_{fg} and c_{bg} are the mean intensities of foreground and background according to the current state of ϕ, and $\lambda_f, \lambda_b, \mu$ are weights of the three energy terms. Both explicit and implicit active contours were implemented in Java in terms of MiToBo[1] operators and ImageJ plugins.

The snake implementation follows the original work of Kass et al. [1], i.e. adopts a combined implicit and explicit gradient-descent technique for solving the PDE, resulting in a linear system of equations to be solved in each iteration. The basic parameters for snake segmentation to be chosen properly are a step size γ for gradient-descent and the preferred length s of each snake segment which is related to the number of snake points used for contour approximation. The segment length is updated in each iteration by contour resampling. Although snakes are not able to change topology during optimization non-simple polygons might occur from self-overlap which are explicitly simplified by polygon tracing. This modifies the segmentation, e.g., intrusions might be removed.

If multiple objects are present in an image, snake segmentation of all objects is done in parallel by concurrently optimizing one snake for each object. To prevent snakes from overlapping a coupling term is added to the energy functional which penalizes snake overlap, however, does not guarantee non-overlapping snakes (see [10] for details).

The implementation of the non-PDE level set optimizer follows [12] with the sequential update scheme, i.e. Gauss-Seidel iteration. If the length term of the CV energy is used. forward differences are used to approximate the gradient of the heaviside function. To preserve topology we adopt the method proposed in [13] for PDE-based minimization which is based on topological numbers. However, we enforce to preserve topology only for the foreground phases (see also [3]).

4. RESULTS

For comparing the two active contour techniques they were each applied to two sets of images originating from different biomedical applications. Below we outline the data and evaluation methods, and provide a comprehensive discussion of qualitative as well as quantitative results.

Test Data The first test set $D1$ consists of microscopy images of scratch assays which are often used for cell motility assessment [3]. Each assay contains a mono layer of U2OS cells in which a scratch is mechanically induced. Subsequently this "wound" is closed by cell migration, which is monitored at different time points to evaluate cell motility. For $D1$, images of 10 cell populations were taken at 7 points in time yielding in total 70 images with scratches showing a large variety in size and shape. The second set $D2$ consists of 8 epifluorescence microscopy images of 57 cells in total with fluorescently labeled focal contacts. For biomedical investigations the number of focal contacts per cell is of interest requiring an accurate extraction of the cell boundaries. Comparison of segmentation results is done qualitatively and quantitatively, given manual ground-truth labelings for both sets. Scratch assays were labeled by two biologist experts and the intersection of their labelings was used as ground-truth, while labelings of one person were available for images of $D2$. Example images from $D1$ and $D2$ are given in Fig. 1.

[1] http://www.informatik.uni-halle.de/mitobo

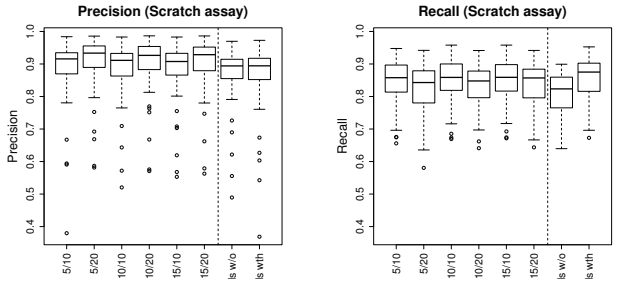


Fig. 2. $\mathcal{R}$ and $\mathcal{P}$ for dataset $D1$. The first six boxes in each plot refer to different snake configurations, the final two refer to level set segmentation without and with post-processing.

Performance Measures For quantitative evaluation we provide recall $\mathcal{R}$ and precision $\mathcal{P}$, where $\mathcal{R} = \frac{TP}{TP+FN}$ and $\mathcal{P} = \frac{TP}{TP+FP}$. TP and FP denote the number of pixels correctly resp. incorrectly segmented as foreground (i.e. scratch or cell area), while FN is the number of ground truth foreground pixels segmented as background. In some experiments parameters were chosen using F-scores defined as $2 \cdot \frac{\mathcal{P} \cdot \mathcal{R}}{\mathcal{P}+\mathcal{R}}$ which is proportional to the Jaccard index used in [5].

Scratch Assays Images For segmenting the images of $D1$ the common CV energy functional [6] with $\lambda_f = \lambda_b = 1$ and $\mu = 0$ is used, i.e. only the CV fitting term is employed. It is, however, applied to an image of local entropies (cf. to [3]). Initially each assay image is smoothed by a Gaussian with $\sigma = 5$, and then for each pixel the local entropy in a window sized 31×31 is calculated. As each image contains one horizontal scratch, the scratch is initialized as a rectangle in the middle of the image spanning 95% of its width and 10% of its height. In addition, as each image contains exactly one scratch topology-preservation is enforced.

In Fig. 1, second column, clips of a prototypical segmentation result for level sets are shown. The scratch boundary is accurately extracted, however, due to topology-preservation intrusions remain which are linked to the cell area by corridors of one pixel width (top). To eliminate these artifacts morphological post-processing by closing with a squared mask of size 3 followed by hole filling is applied (see Fig. 1).

In Fig. 2 box plots of $\mathcal{R}$ and $\mathcal{P}$ for both segmentations are shown. Level set segmentation results in a median $\mathcal{R}$ of 0.8234 and a median $\mathcal{P}$ of 0.8941. As expected, removing intrusions yields a distinctly higher median $\mathcal{R}$ of 0.8751, where median $\mathcal{P}$ is barley affected as scratch boundaries are not expanded and, thus, no new FP are introduced.

Applying snakes suitable configuration parameters are required, i.e. segment length s and step size γ, and a suitable termination criterion needs to be applied. In all cases optimization was stopped at iteration t if the smoothed relative change in snake area between $t-5$ and $t-15$ dropped below 0.001. To find suitable s and γ, segmentation was accomplished with different combinations of parameters, i.e. $\gamma \in \{5, 10, 15\}$ and $s \in \{10, 20\}$. The left six boxes in each plot of Fig. 2 summarize the results. On the one hand larger s, which result in a coarser contour approximation, increase $\mathcal{P}$ about 0.0180 on average, and lead to a slight decrease in $\mathcal{R}$ of -0.0092 on average. On the other hand the step size γ does not appear to have significant influence as the median $\mathcal{P}$ for all segment lengths lie in ranges of 0.9117 ± 0.0040 and 0.9299 ± 0.0035, respectively. Likewise the median $\mathcal{R}$ for constant segment length are in the ranges of 0.8584 ± 0.0006 and 0.8500 ± 0.0070. For subsequent comparisons the parameters $\gamma = 5$ and $s = 10$ resulting in the largest median F-score were used. Exemplary results are given in Fig. 1 (left). Post-processing is not required for snakes due to polygon simplification which removes intrusions as explicitly done via post-processing for level sets (cf. Sec. 3).

The quantitative results for snake segmentation suggest to favor smaller snake segments to achieve higher $\mathcal{R}$. This is particularly true if objects with very ragged contours are to be segmented, like the scratch contours. There are numerous examples in the test images where only the use of smaller segments allows for concavities to be properly segmented. Note, however, that computational costs increase with decrease of s as this results in larger numbers of polygon points.

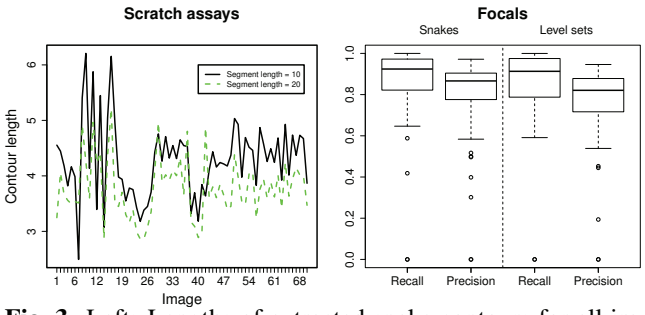


Fig. 3. Left: Lengths of extracted snake contours for all images of data set $D1$ are for $s = 10$ and $s = 20$, respectively. Right: Box plots of $\mathcal{R}$ and $\mathcal{P}$ the snake and level set segmentations of the cell images in data set $D2$.

Another interesting observation results from correlating the segment length s with the overall length of final contours. As can be seen in Fig. 3, left, there is an obvious tendency of snakes with larger segments to yield shorter object contours. Accordingly, by varying segment length an implicit length regularizer is introduced into snake segmentation.

A direct comparison of the F-scores for snake (0.8828) and level set segmentation (0.8868) does not induce a clear tendency towards either of the two techniques. Level sets tend to yield higher $\mathcal{R}$ while snakes result in larger $\mathcal{P}$. But, there is a significant difference regarding the computational effort of both approaches. While the median processing time for level sets is 118s with a maximum of 241s, the median for the snakes is 540s with a maximum of 49min. In each snake iteration the new set of snake points is calculated by solving a linear system of equations containing twice as many variables as snake points, thus, the computation time is directly related to the number of snake points and increases with growing

contour length and decreasing s. Also smaller γ often coincide with higher computation times. For level sets the effort of each iteration depends on the number of contour pixels due to topology preservation which is directly related to the compactness of the object region. Elongated structures require more iterations than compact ones.

Cell Images To segment the borders of individual cells in the images of $D2$ again the CV fitting energy is used. For preprocessing the images are smoothed by Gaussian with $\sigma = 4$ which blurs the focal contacts' intensities.

Adopting snakes for segmentation a parameter ratio of $\frac{\lambda_f}{\lambda_b} = \frac{1}{150}$ was chosen for the CV energy, and in addition a snake overlap penalty was applied with a weight of 0.6 relative to the CV term. As termination criterion a maximum of 700 iterations was used, or alternatively a relative change in area between two iterations of not more than 0.001. Considering again F-scores a segment length of $s = 5$ and a step size of $\gamma = 2$ turned out to be favorable, yielding a median $\mathcal{R}$ of 0.9241 and a median $\mathcal{P}$ of 0.8663.

Using level sets with the same CV fitting term proper segmentation was impossible due to missing regularization. This reflects the sensitivity to noise as also observed, e.g., in [15]. It seems that the implicit length regularizer hypothesized above allows snakes to successfully segment objects in absence of an explicit regularizer. These findings show that the same energy does not necessarily lead to comparable results on the same data when used with implicit active contours compared to explicit ones as might have been expected.

These shortcoming of the level sets were overcome including the length penalty term of the CV energy into the functional, i.e. setting $\mu = 2000$. Box plots of quantitative segmentation results are shown in Fig. 3. For level sets a median $\mathcal{R}$ of 0.9130 and a median $\mathcal{P}$ of 0.8207 is observed, resulting in a median F-score of 0.8502 compared to 0.8775 for snake segmentation. However, as can also be seen from the qualitative segmentation results in Fig. 1 (right), the differences are marginal. Again it is difficult to favor one of the techniques, provided parameters are properly chosen for each technique. The main difference between snakes and level sets is again computational effort. The median time for level sets is $30s$ and 1014s for snake segmentation.

5. CONCLUSION

Using the same energy functional, snakes and non-PDE level sets achieve comparable results of high-quality. But, regarding implementation details, necessity for data pre- and post-processing, and computational effort there are distinct differences. Particularly our findings support the conjecture that snakes incorporate an implicit length penalty varying with the segment length. Depending on the application each of both representations may have advantages, and knowing their specifics is essential for chosing the adaquate representation.

6. REFERENCES

[1] M. Kass, A. Witkin, and D. Terzopoulos, "Snakes: Active contour models," *IJCV*, vol. 1, pp. 321–331, 1988.

[2] S. Osher and J.A. Sethian, "Fronts propagating with curvature-dependent speed: algorithms based on hamilton-jacobi formulations," *Journal of Computational physics*, vol. 79, no. 1, pp. 12–49, 1988.

[3] M. Glaß et al., "Scratch assay analysis with topology-preserving level sets and texture measures," in *Proc. IbPRIA*, Gran Canaria, 2011, pp. 100–108.

[4] B. Möller et al., "MiCA - easy cell image analysis with normalized snakes," in *MIAAB*, K. Rohr, Ed., 2011.

[5] L. He et al., "A comparative study of deformable contour methods on medical image segmentation," *Image and Vision Comp.*, vol. 26, no. 2, pp. 141 – 163, 2008.

[6] T.F. Chan and L.A. Vese, "Active contours without edges," *IEEE T-IP*, vol. 10, no. 2, pp. 266–277, 2001.

[7] T. McInerney et al., "T-snakes: Topology adaptive snakes," *Med. Image Anal.*, vol. 4(2), pp. 73–91, 2000.

[8] N. Ray et al., "Active contours for cell tracking," in *Proc. of 5th IEEE Southw. Symp. on Image Analysis and Interpretation*, Washington, DC, USA, 2002, p. 274 ff.

[9] H. Shen et al., "Automatic tracking of biological cells and compartments using particle filters and active contours," *Chemometrics and Intelligent Laboratory Systems*, vol. 82, no. 1-2, pp. 276–282, May 2006.

[10] C. Zimmer et al., "Coupled parametric active contours," *IEEE T-PAMI*, vol. 27, no. 11, pp. 1838–1842, 2005.

[11] D.J. Williams and M. Shah, "A fast algorithm for active contours and curvature estimation," *CVGIP: Image Underst.*, vol. 55, pp. 14–26, January 1992.

[12] B. Song and T. Chan, "A fast algorithm for level set based optimization," *UCLA Cam Report 02-68*, 2002.

[13] X. Han, C. Xu, and J.L. Prince, "A topology preserving level set method for geometric deformable models," *IEEE T-PAMI*, vol. 25, no. 6, pp. 755–768, 2003.

[14] D.P. Mukherjee, N. Ray, and S.T. Acton, "Level set analysis for leukocyte detection and tracking," *IEEE T-IP*, vol. 13, no. 4, pp. 562–572, 2004.

[15] O. Dzyubachyk et al., "Advanced level-set-based cell tracking in time-lapse fluorescence microscopy," *IEEE T-MI*, vol. 29, no. 3, pp. 852 –867, march 2010.

[16] A. Dufour et al., "Segmenting and tracking fluorescent cells in dynamic 3-D microscopy with coupled active surfaces," *IEEE T-IP*, vol. 14(9), pp. 1396–1410, 2005.